Acta Crystallographica Section A
Foundations of Crystallography
ISSN 0108-7673

Received 17 March 2004
Accepted 13 July 2004

Synchrotron charge-density studies in materials chemistry: 16 K X-ray charge density of a new magnetic metal-organic framework material, $[Mn_2(C_8H_4O_4)_2(C_3H_7NO)_2]$

R. D. Poulsen,[a] A. Bentien,[a] T. Graber[b] and B. B. Iversen[a]*

[a]Department of Chemistry, University of Aarhus, DK-8000 Århus C, Denmark, and [b]University of Chicago, IL 60637, USA. Correspondence e-mail: bo@chem.au.dk

A new magnetic metal-organic framework material, $[Mn_2(C_8OH_{44})_2(C_3H_7NO)_2]$, has been synthesized. The structure consists of chains of carboxylate-bridged Mn atoms interconnected with acid linkers, giving much larger interchain than intrachain Mn···Mn distances. Magnetic susceptibility data fitted to a Curie–Weiss law give $\Theta = -5.7$ K and a total magnetic moment of 5.96 μ_B. The heat capacity provides no evidence of magnetic ordering down to 2 K. The X-ray charge density was determined from multipole modeling of 16 (1) K single-crystal synchrotron-radiation data. The structural surroundings of the two unique Mn centers are different, but orbital population analysis reveals close to single electron occupation in all 3*d* orbitals of both Mn sites, in agreement with the magnetic susceptibility measurements. Bader topological analysis shows the presence of direct chemical Mn···Mn interactions only in two out of three intrachain contacts, which suggests a 'broken' chain. The topological measures and approximate energy densities at the metal–ligand bond critical points (ρ, $\nabla^2\rho$, G, V and H) indicate ionic interactions. Formal electron counting suggests mixed-valence Mn sites, but this hypothesis is not supported by the Bader atomic charges [q(Mn) = +2.035 and +2.031].

1. Introduction

The study of chemical bonding is a cornerstone in chemistry. One of the most effective methods for studies of chemical bonding is analysis of the distribution of charge in space, and this method forms a main rationale for the X-ray charge-density (CD) field (Coppens, 1997). During the past ten years, a number of exciting advances have occurred in the X-ray CD field, including the development of reliable helium-based cooling devices, and the availability of intense short-wavelength synchrotron radiation and area-detector technology (Iversen *et al.*, 1999). In addition, the introduction of new interpretation tools, such as topological analysis, has produced substantial new understanding of chemical bonding (Bader, 1994).

After a slow start, the number of synchrotron charge-density studies is now increasing rapidly. Synchrotron radiation offers clear advantages relative to conventional sources, because data of higher accuracy can potentially be collected when systematic errors such as absorption, extinction and anomalous scattering are reduced (Iversen *et al.*, 1999). Coppens *et al.* (2004) have recently reviewed the present state of affairs with regard to synchrotron CD studies. The many different types of complex materials now being studied with synchrotron radiation are a testimony to a maturing research field, which is ready to enter mainstream chemistry. With synchrotron radiation, only minute crystal specimens are needed, thus increasing enormously the number of systems available for CD studies. We have during the past decade carried out synchrotron CD studies on a wide range of materials, based on measurements performed at beamline X3A1 at NSLS, USA (Iversen *et al.*, 1998; Macchi *et al.*, 2001, Overgaard *et al.*, 2001, 2002, 2003). These efforts are now being shifted to the Advanced Photon Source in Chicago, where the ChemMatCARS beamline is being utilized for accurate crystallographic and CD studies. In the present paper, we present our first synchrotron CD study from this exciting new facility and document the fact that high-quality data can be measured for complex molecular systems of great current interest.

One of the foundations of materials chemistry is the determination of structure–property relations for a given class of materials. The immense progress in experimental CD methods now makes it possible to determine quickly the CDs even of complex materials containing heavy atoms. Ultimately, this capability can revolutionize materials chemistry, since

much stronger correlations can be derived on the basis of CDs (orbital populations, atomic charges, topological bonding measures *etc.*) rather than merely the atomic connectivity (Overgaard *et al.*, 2003). We report here the first step in such a process by determining the CD of a new magnetic metal-organic framework (MOF) structure, $[Mn_2(C_8H_4O_4)_2(C_3H_7NO)_2]$ (Fig. 1). This compound is one in a series of structurally related new magnetic MOF materials synthesized in our laboratory (Poulsen *et al.*, 2004). There has been an explosion of interest in MOF systems (O'Keeffe *et al.*, 2000; Edgar *et al.*, 2001; Noro *et al.*, 2002; Kitaura *et al.*, 2003), and recent highlights include nanoporous systems based on Zn centers coordinated by various dicarboxylate linkers to form cubic host structures (Eddaoudi *et al.*, 2002; Rosi *et al.*, 2003; Yaghi *et al.*, 2003). By variation of the length of the acid linker, incremental increases in pore sizes over a large range have been achieved, and some of these compounds exhibit very high capacity for gas storage. However, our interest in MOFs concerns magnetic properties (Miller & Epstein, 1995; Price *et al.*, 2001). The 'LEGO' molecular building block approach in MOFs may provide novel systems for fundamental studies of magnetic exchange mechanisms. Since the organic linker molecules potentially can be incrementally increased in length as well as being designed with specific electronic properties, it may be possible to fine-tune the magnetic interaction pathways between the metal centers. Contrary to many of the previously reported MOFs, solvent molecules in $[Mn_2(C_8H_4O_4)_2(C_3H_7NO)_2]$ do not occupy open cavities but are coordinated directly to the Mn atoms, creating a crystalline system without structural disorder at 16 (1) K. It is therefore possible to determine experimentally not only the detailed very low temperature crystal structure but also an accurate X-ray charge density.

2. Experimental

2.1. Synthesis

The synthesis of the metal-organic framework $[Mn_2(C_8H_4O_4)_2(C_3H_7NO)_2]$ is a *one pot* reaction. A mixture of benzene dicarboxylic acid (BDC; 0.332 g, 2 mmol) and dimethylformamide (DMF; 6 ml) was added in an autoclave to $Mn(NO_3)_2\cdot 6H_2O$ (0.574 g, 2 mmol) dissolved in DMF (5 ml). The mixture was kept at 381 K for 18 d. The crystals have the same shape as the monoclinic unit cell and are not resistant to exposure to air.

2.2. Physical properties

The total heat capacity (C_p) and magnetic susceptibility (χ) were measured on a Quantum Design PPMS system at the Department of Chemistry, University of Aarhus, from 2 to 400 K on a pellet pressed from finely ground powder. Thermogravimetric analysis (TGA) and differential thermal analysis (DTA) were carried out from 298 to 833 K using a Stanton-Redcroft TGA–DTA simultaneous thermal analyzer STA 1000/1500. A heating rate of 10 K min^{-1} was applied in an Ar gas flow.

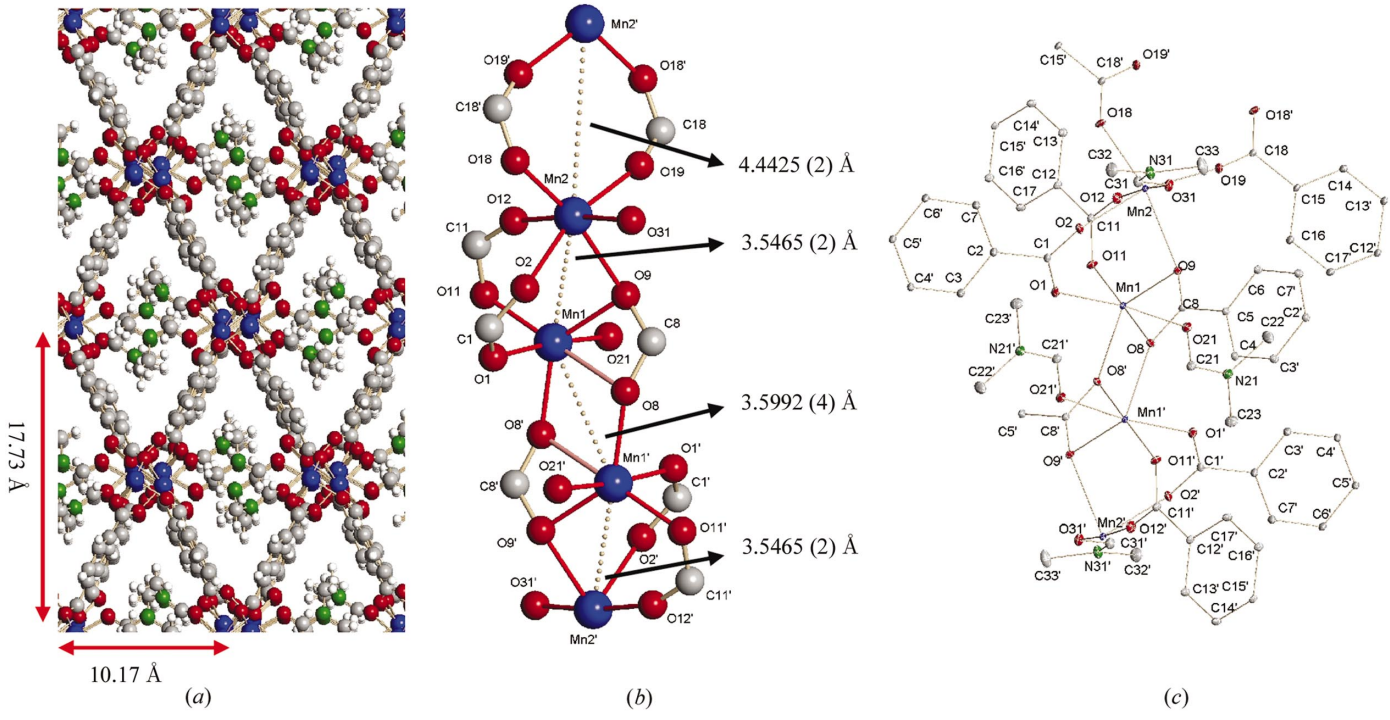

Figure 1
The crystal structure of $[Mn_2(C_8H_4O_4)_2(C_3H_7NO)_2]$ at 16 (1) K. (*a*) The crystal structure along the *a* axis. The DMF molecules bonded to Mn occupy the voids. (*b*) The Mn chain interconnected by carboxylate groups. (*c*) The atom connectivity, with displacement ellipsoids shown at the 50% probability level. H atoms have been omitted for clarity

2.3. X-ray data collection

A minute colorless single crystal ($0.020 \times 0.020 \times 0.025$ mm) was mounted in protective oil on a glass fiber rod glued to a small copper wire. This assembly was mounted on a brass pin, which was placed on the goniometer of a Huber four-circle diffractometer at the ChemMatCARS beamline at the Advanced Photon Source, Argonne National Laboratory. The crystal was cooled to 16 (1) K using the cold He stream of a Pinkerton-type cooling device (Hardie *et al.*, 1998). Data collection was performed in φ-scan mode, with steps of 0.1° (1 s exposure) and fixed ω and χ angles. The diffracted intensity was recorded with a Bruker 6000 CCD detector mounted on the 2θ arm of the diffractometer. The detector was placed at a distance of 7.32 cm from the crystal, with $\theta = 28°$. This set-up gives a maximum resolution of 1.17 Å^{-1} for the data set. The data collection time was 13 h. In total, 99 808 reflections were integrated with *SAINT-Plus* (Sheldrick, 2003), and were subsequently absorption corrected and averaged with *SORTAV* (Blessing, 1997). Note that the use of a very small crystal in combination with high-energy synchrotron radiation has virtually removed absorption effects in the data (see Table 1). After integration, the data were corrected for oblique incidence into the CCD detector (Wu *et al.*, 2002), and a φ correction was performed with *SADABS* (Sheldrick, 2003). In further analysis of the data, only reflections measured more than twice were included in the refinements ($n_{\rm meas} > 2$). In previous synchrotron area-detector studies, we have observed that redundancy in the data is the key to accuracy, since this approach, for example, facilitates removal of outliers in the data (Iversen *et al.*, 1999). Further experimental details are listed in Table 1.

2.4. Multipole refinement

The structure was solved from the diffraction data using the direct methods program in *SHELXTL* (Sheldrick, 2003). All H atoms were placed in calculated positions using standard neutron data for C—H distances (Fig. 1). Disorder of the coordinated solvent molecules has been observed for similar

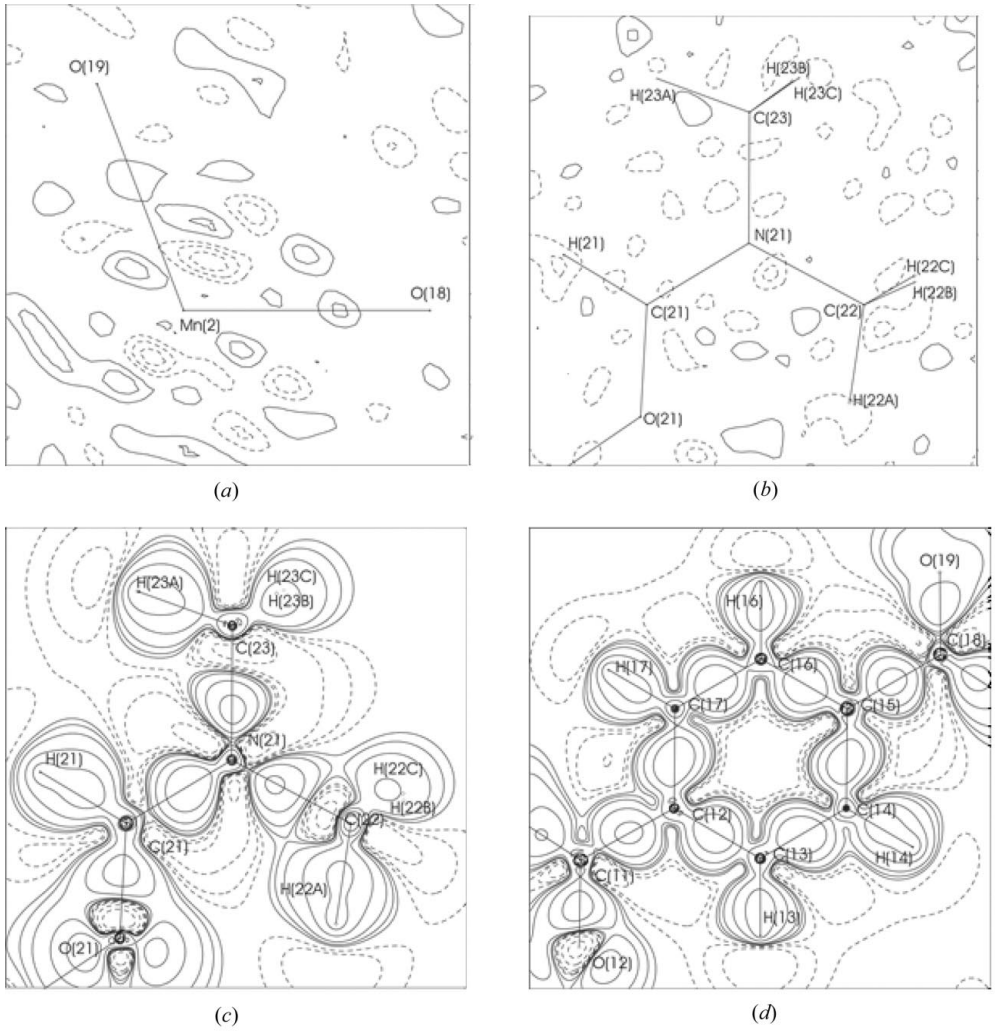

Figure 2
Residual density in the (*a*) Mn(2)/O(18)/O(19) plane and (*b*) C(21)/C(22)/C(23) plane of the DMF ligand bonded to Mn(1). (*c*) and (*d*) show the static deformation density in the C(21)/C(22)/C(23) plane of the DMF ligand bonded to Mn(1) and of a benzene ring of a BDC linker molecule, respectively. The contour level is 0.1 e Å^{-3}. Solid lines are positive and dashed lines are negative.

Table 1
Crystallographic and experimental details for $C_{22}H_{22}Mn_2O_{10}$.

Space group†	$P2_1/c$
Formula weight (g mol^{-1})	584.3
T (K)	16 (1)
a (Å)	13.396 (2)
b (Å)	10.172 (2)
c (Å)	17.725 (2)
β (°)	90.090 (5)
V (Å^3)	2415 (1)
λ (Å)	0.420
Z	4
ρ_{calc} (Mg m^{-3})	1.607
μ_l (mm^{-1})	0.224
T_{max}, T_{min}	0.997, 0.992
Data collection time (h)	13
Integrated reflections	99 808
R_{int} (all reflections)	0.0471
Unique reflections ($n_{meas} > 2$)	18 127
$(\sin\theta/\lambda)_{max}$ (Å^{-1})	1.17
N_{par}	897
N_{obs} (2σ)	12180
$R(F)$, $R(F^2)$	0.0222, 0.0318
$R_w(F)$, $R_w(F^2)$	0.0227, 0.0450
Goodness of fit	0.7102

† The β angle of 90.090 (5)° is close to 90° (orthorhombic structure), but systematic absences and intensity symmetry provide a conclusive assignment of the monoclinic space group.

MOFs, such as $[Mn_3(C_8H_4O_4)_3(C_5H_{11}NO)_2]$ (Poulsen *et al.*, 2004), but no disorder of the two DMF molecules is observed in the structure of $[Mn_2(C_8H_4O_4)_2(C_3H_7NO)_2]$ at 16 (1) K. The initial structural model (atom positions and thermal motion) was obtained from a high-order refinement of data with $\sin\theta/\lambda > 0.8$ Å^{-1}. This structural model was kept fixed during the initial multipole refinements with *XD* (Koritsanszky *et al.*, 2002). The complexity of the refinement was gradually increased over a series of refinements, and the final multipole model included hexadecapoles on Mn atoms, octupoles on all other non-H atoms, and one monopole and one bond-directed dipole for all H atoms. Mn^{2+} radial functions were used for the Mn atoms, from the SCM scattering factor bank in *XD*. Three κ parameters were introduced on each metal site, in the form of one monopole κ' {κ'[Mn(1)] = 0.955 (7) and κ'[Mn(2)] = 0.973 (7)} and two valence κ'' parameters {κ''[Mn(1), even poles] = 0.74 (3), κ''[Mn(1), odd poles] = 1.23 (11), κ''[Mn(2), even poles] = 0.67 (2) and κ''[Mn(2), odd poles] = 0.989 (2)}. For all other heavy atoms, the two standard κ' and κ'' parameters were refined for each chemically unique type of atom [κ'(N) = 0.964 (7), κ''(N) = 0.88 (5), κ'(C) = 0.949 (3) and κ''(C) = 0.865 (9)]. For the O atoms, a $\kappa' = \kappa''$ [= 0.966 (2)] constraint was imposed to prevent the valence functions becoming very diffuse. In the final refinement, both structural and electronic parameters were varied simultaneously, giving a total of 897 parameters against 12180 observations [$I > 2\sigma(I)$]. The Hirshfeld rigid-bond test was fulfilled satisfactorily, with a mean value of Δ_{A-B} of 10 pm^2 (Harel & Hirshfeld, 1975; Hirshfeld, 1976). Plots of the residual density in the central regions show no significant features. Fig. 2(*a*) shows the worst plane, with a residual of around 0.3 e Å^{-3} near the Mn(2) site. In the ligand and linker molecule regions, the residual is typically below 0.1 e Å^{-3} (Fig. 2*b*). The low residual density in the DMF regions confirms that at 16 K there is no disorder in the structure. The corresponding static deformation densities show the expected features for the organic units (Figs. 2*c* and 2*d*), thus confirming that a reliable multipole model has been obtained.

3. Results and discussion

3.1. Physical properties

Fig. 3 shows the magnetic susceptibility (χ) measured between 2 and 400 K. A fit of the data above 10 K to a Curie–Weiss law [$\chi = C/(T - \Theta)$, with $C = N\mu_0\mu_B^2\mu_{eff}^2/(3k_B)$] gives $\Theta = -5.7$ K and an effective moment of 5.96 μ_B, in excellent agreement with the theoretical value of 5.9 for a free Mn^{2+} ion (Ashcroft & Mermin, 1976). However, the magnetic susceptibility is a macroscopic property, which does not reveal the detailed atomic origin of the magnetism in the structure. Thus no distinction is made between the two structurally very different Mn sites, nor is there consideration of covalence in the bonding, which can limit the validity of the model with magnetism centered only on Mn sites. The lower inset of Fig. 3 shows that the magnetization per Mn atom does not reach saturation in magnetic fields of up to 5 T (at 2 K). The negative Curie temperature suggests antiferromagnetic fluctuations, but the measured heat capacity does not provide any evidence for magnetic ordering down to 2 K (upper insert of Fig. 3). The broad anomaly observed in the heat capacity (C_p) between 30 and 100 K may originate from structural ordering of the DMF molecule. Indeed, at 100 K, rotational disorder in one of the DMF methyl groups is observed (data not shown).

The thermal stability of the material was examined through simultaneous TGA and DTA analysis (see supporting information[1]). The material is thermally inert up to ~433 K, where a 10–12% mass loss, which corresponds approximately to the mass of one DMF molecule, is observed. Another thermal effect is observed at 573 K, where the material loses another 10% of the mass. Finally, complete decomposition sets in above ~773 K. Thus it appears that the two unique DMF ligands extending into the network cavity are lost in two steps, whereas the network decomposes above 773 K.

3.2. Structure and electron density

The structure of the metal-organic framework of $[Mn_2(C_8H_4O_4)_2(C_3H_7NO)_2]$ consists of chains of carboxylate-bridged Mn atoms interconnected by the acid linker, giving much larger interchain than intrachain Mn···Mn distances (Fig. 1). The direction of the Mn rows is along the *a* axis and there appears to be a unique magnetic direction along the chains. Both Mn atoms have distorted octahedral environments, atom Mn(2) being closer to ideal octahedral coordi-

[1] Supplementary data for this paper including a crystallographic information file (CIF) containing tables of refined multipole parameters, a table of topological properties of the non-H-atom bonds and thermal analysis data are available from the IUCr electronic archives (Reference: XC5018). Services for accessing these data are described at the back of the journal.

nation than Mn(1) (see supporting information). The coordination of atom Mn(1) resembles more a trigonal bipyramid, where one extra bond [Mn(1)—O(8)] has been inserted into the pyramidal plane (Fig. 1*c*). In Table 2, the Mn—O bond lengths are listed; full structural details are given in the supporting information. None of the acid groups show significant localization of the negative charge, the C—O bond lengths ranging from 1.261 (1) to 1.273 (1) Å. Thus, acid O atoms coordinated to one Mn atom formally have a charge of −0.5 e. Formal charge counting for the Mn atoms then gives Mn(1) = +1.75 e and Mn(2) = +2.25 e, when acid O atoms bridging two Mn atoms are counted as −0.25 e. From the synthesis, we would expect a +2 valence state on the metal since an Mn^{2+} source is used and there are no obvious oxidation or reduction pathways. It is interesting if the experimental charge distribution confirms the formal mixed valence.

Fig. 4 shows the Laplacian distribution in selected planes. The DMF ligand and BDC linker molecules show expected features corresponding to the static deformation densities shown in Fig. 2. The Mn sites appear spherical, which indicates an even distributions of electrons in the 3*d* orbitals. In Table 3, the Mn 3*d* orbital populations derived from the refined multipole parameters are listed (Holladay *et al.*, 1983; Sabino & Coppens, 2003). The values show that both Mn atoms are indeed in high-spin states, with approximately one electron in each *d* orbital. Thus the simple picture of a spherical Mn^{2+} ion is actually quite accurate in this compound. The substantial structural differences between the two Mn sites do not seem to have a large effect on the 3*d* populations.

In Table 2, topological properties of the Mn···Mn and Mn—O bond critical points are listed. The topological results for the ligand bonds are given in the supporting material. There are bond critical points (b.c.p.) for Mn(1)···Mn(1′) [3.5992 (4) Å] and Mn(2)···Mn(2′) [4.4425 (2) Å] but not Mn(1)···Mn(2) [3.5465 (2) Å]. It is strange that it is not the longest Mn···Mn interaction [Mn(2)···Mn(2′); Fig. 1*b*] that lacks the b.c.p. Between atoms Mn(1) and Mn(2), we locate a ring critical point (r.c.p.) with a density of $\rho = 0.036$ e Å^{-3} ($\lambda_1 = -0.09$, $\lambda_2 = 0.16$, $\lambda_3 = 0.54$). This r.c.p. has a larger density than the b.c.p. of the Mn(2)···Mn(2′) interaction ($\rho = 0.014$; Table 2). When examining the eigenvalues of the Mn(1)···Mn(1′) (−0.19, −0.01, 1.28) and Mn(2)···Mn(2′) (−0.03, −0.01, 0.29) b.c.p.s it is clear that the significance of the negative eigenvalues is questionable, and only slight changes in the density could result in these b.c.p.s changing to r.c.p.s. This important aspect will be further addressed with *ab initio* theoretical calculations. However, if there is direct chemical interaction between some of the metals, but not continuously along the Mn chain, then the interruption of the chain may be responsible for the lack of complete antiferromagnetic ordering in the structure. The antiferromagnetic fluctuations observed in the susceptibility data may be caused, for example, by ordering of the Mn(1)···Mn(1′) and Mn(2)···Mn(2′) pairs but not by complete ordering along the chain. Since the *d* orbitals responsible for the magnetism are localized and we indeed observe limited metal–ligand orbital interaction in the present compound, it seems that direct Mn···Mn *d*-orbital overlap is unlikely. Several studies have examined metal–metal interactions in molecular complexes (Bianchi *et al.*, 2000; Macchi & Sironi, 2003). The topological values at the Mn···Mn bond critical points of the present three-dimensional network structure are similar to those reported in molecular complexes, but a quantitative comparison will be postponed until data are available for the other network compounds in the present series.

The density at the Mn—O b.c.p.s ranges from 0.133 (2) to 0.410 (6) e Å^{-3}, and all Laplacian values are positive and increase with decreasing Mn—O distance. This behavior has also been observed in Fe—O interactions in carboxylate-bridged polynuclear complexes as well as in hydrogen bonds (Overgaard *et al.*, 2003; Espinosa *et al.*, 2002). For all Mn—O

Table 2
Topological properties at the metal–ligand bond critical points.

D_{ij} is the refined internuclear distance (Å), whereas R_{ij} is the sum of the distances from the bond critical point to the attractors (Å). ρ is the electron density (e Å^{-3}) and $\nabla^2\rho$ is the Laplacian (e Å^{-5}). G, V and H are the kinetic energy density, the potential energy density and the total energy density, respectively (Hartree Å^{-3}). The energy densities are calculated from the Abramov (1997) functional.

Bond	D_{ij}	R_{ij}	ρ	$\nabla^2\rho$	G	V	H	G/ρ
Mn(1)···Mn(1)	3.5992 (4)	3.5992	0.063 (1)	1.073 (1)	0.06	−0.04	0.02	0.92
Mn(2)···Mn(2)	4.4425 (2)	4.4425	0.014 (1)	0.244 (0)	0.01	−0.01	0.01	0.86
Mn(1)—O(1)	2.1026 (10)	2.1080	0.410 (6)	8.153 (8)	0.56	−0.55	0.01	1.37
Mn(1)—O(8)	2.4668 (9)	2.4850	0.133 (2)	3.036 (3)	0.17	−0.13	0.04	1.27
Mn(1)—O(9)	2.2178 (9)	2.2209	0.309 (4)	5.934 (6)	0.39	−0.37	0.02	1.26
Mn(1)—O(11)	2.1183 (9)	2.1217	0.336 (5)	8.083 (7)	0.51	−0.45	0.06	1.51
Mn(1)—O(21)	2.1723 (10)	2.1787	0.330 (5)	6.783 (6)	0.44	−0.41	0.03	1.34
Mn(1)—O(8′)	2.1484 (7)	2.1522	0.307 (5)	7.352 (7)	0.46	−0.40	0.06	1.48
Mn(2)—O(2)	2.1945 (8)	2.1991	0.345 (5)	6.127 (6)	0.42	−0.42	0.01	1.22
Mn(2)—O(9)	2.3637 (8)	2.3673	0.212 (3)	3.754 (4)	0.24	−0.21	0.03	1.11
Mn(2)—O(12)	2.1592 (8)	2.1698	0.347 (5)	6.260 (7)	0.43	−0.42	0.01	1.24
Mn(2)—O(18)	2.1383 (9)	2.1500	0.359 (5)	6.926 (7)	0.47	−0.45	0.02	1.31
Mn(2)—O(19)	2.1056 (9)	2.1165	0.382 (6)	7.149 (8)	0.50	−0.49	0.01	1.30
Mn(2)—O(31)	2.2092 (8)	2.2209	0.317 (4)	6.041 (6)	0.40	−0.38	0.02	1.26

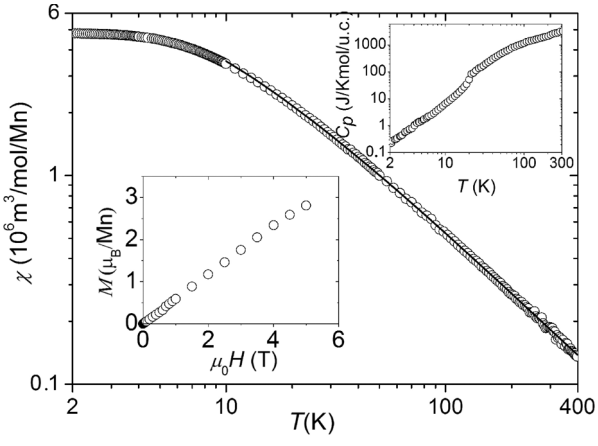

Figure 3
Magnetic susceptibility (χ) per Mn atom as a function of temperature (T). The solid line is a fit to a Curie–Weiss law. The lower inset shows the magnetization (M) per Mn atom measured at 2 K in magnetic fields ($\mu_0 H$) up to 5 T. The upper inset shows the total heat capacity (C_p).

Table 3
Orbital populations derived from the refined multipole parameters (Holladay *et al.*, 1983; Sabino & Coppens, 2003).

For Mn(1), the *x* axis points towards O(9) and the *y* axis towards O(11). For Mn(2), the *x* axis points towards O(9) and the *y* axis towards O(2). Thus, for both Mn atoms, the *z* axes are approximately towards the DMF ligands. The first number is the refined number of electrons and the second number the relative population in %.

Orbital	Mn(1)	Mn(2)
d_{z^2}	1.03 (4), 21%	1.13 (4), 23%
$d_{x^2-y^2}$	1.13 (4), 23%	1.09 (4), 22%
d_{xz}	0.80 (4), 16%	0.76 (4), 15%
d_{yz}	0.94 (4), 19%	1.02 (4), 21%
d_{xy}	1.01 (4), 21%	0.90 (4), 18%
Total	4.91	4.90

bonds, the total energy density (H) is close to zero and G/ρ is fairly large. The topological measures indicate ionic metal–ligand interactions (Macchi & Sironi, 2003), which further corroborates the qualitative bonding picture obtained from the magnetic measurements and the Mn *d*-orbital populations.

It is interesting to examine whether the formal mixed valence of the Mn sites is reflected in the experimental CD. In Table 4, Bader atomic charges derived from the experimental CD are listed. For comparison, the atomic charges derived from the refined monopole parameters are also given. The Bader charges of the Mn atoms reflect, much better than the monopole charges, the formal chemistry. The two Mn atoms have almost identical charges and total volumes, even though the coordination around these atoms is quite different. In Fig. 5, the zero flux surfaces of the two Mn atoms are shown. The volume of atom Mn(1) is more oddly shaped than that of atom Mn(2), which is almost cubic. Even so, the dipole moments (Table 4), and even the quadrupole moments (data not shown), are very similar, suggesting that the important parts of the charge distribution are relatively close to the nucleus, and that the low-density regions near the atomic surface play minor roles in determining the atomic properties.

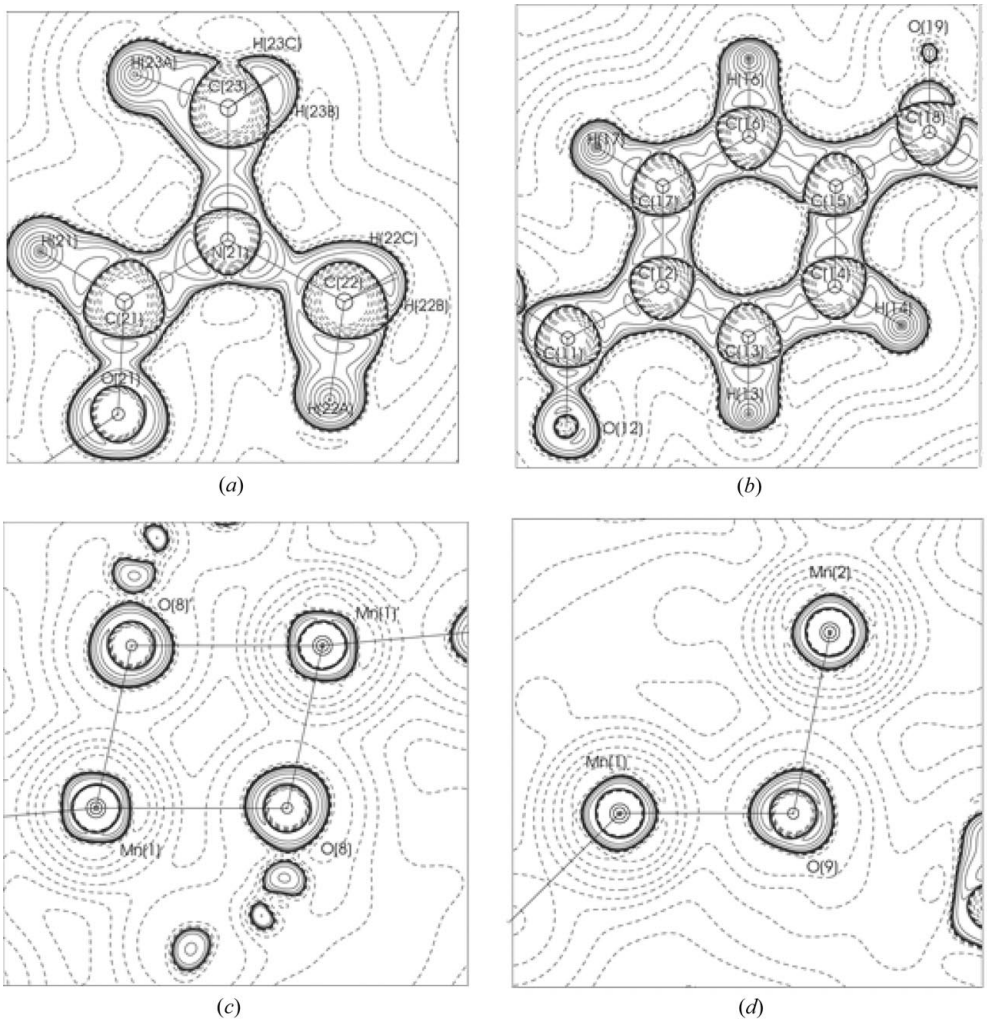

(*a*) (*b*) (*c*) (*d*)

Figure 4
Laplacian distributions in (*a*) the C(21)/C(22)/C(23) plane of the DMF ligand bonded to Mn(1), (*b*) the benzene ring of a BDC linker molecule, (*c*) the Mn(1)/O(8)/Mn(1′) plane and (*d*) the Mn(1)/O(9)/Mn(2) plane. The contour level is $2^x10^{\pm y}$ (x = 1, 2 and 3; y = 0, 1, 2 and 3). Solid lines are negative contours and dashed lines are positive.

Table 4
Atomic properties as defined within the quantum theory of atoms in molecules (Bader, 1994).

	Monopole charge (e)	Bader charge (e)	V_{Total} (Å^3)	Dipole moment
Mn(1)	+0.10 (5)	+2.04	69.2	0.09
Mn(2)	+0.11 (4)	+2.03	68.1	0.03
O(1)	−0.19 (4)	−1.15	111.9	0.59
O(2)	−0.24 (4)	−1.25	111.3	0.65
O(8)	−0.24 (4)	−1.13	99.5	0.54
O(9)	−0.26 (4)	−1.17	100.6	0.64
O(11)	−0.34 (4)	−1.25	108.2	0.57
O(12)	−0.26 (4)	−1.20	117.7	0.68
O(18)	−0.22 (4)	−1.25	120.7	0.64
O(19)	−0.29 (4)	−1.26	120.1	0.61
O(21)	−0.26 (4)	−1.30	121.4	0.60
O(31)	−0.34 (4)	−1.45	122.5	0.66

The fact that both Mn atoms have small dipole moments again reflects the even distribution of electrons in the *d* orbitals.

There appear to be subtle differences among the atomic properties of the O atoms. However, these differences are difficult to quantify on the basis of the limited data available. As for the metal–metal interactions, the structural origin and consequences of the oxygen differences will be further addressed when CD data for the other members of this series of MOF materials are available.

4. Conclusions

The present study demonstrates that high-quality, very low temperature, synchrotron CDs can be obtained quickly (*e.g.* in hours) on complex heavy-atom materials. The new magnetic MOF material $[Mn_2(C_8H_4O_4)_2(C_3H_7NO)_2]$ shows antiferromagnetic fluctuations but does not reach magnetic ordering down to 2 K. The CD analysis suggests an interrupted Mn chain, which lacks direct bond critical points in one of the three unique Mn···Mn contacts. However, because of the low density at the Mn···Mn bond critical points, the significance of the curvatures is questionable and thus the nature of the critical points is somewhat uncertain. We are currently analyzing CD data from related Mn-based MOF structures in order to gain increased understanding of their physical properties through comparative CD analysis.

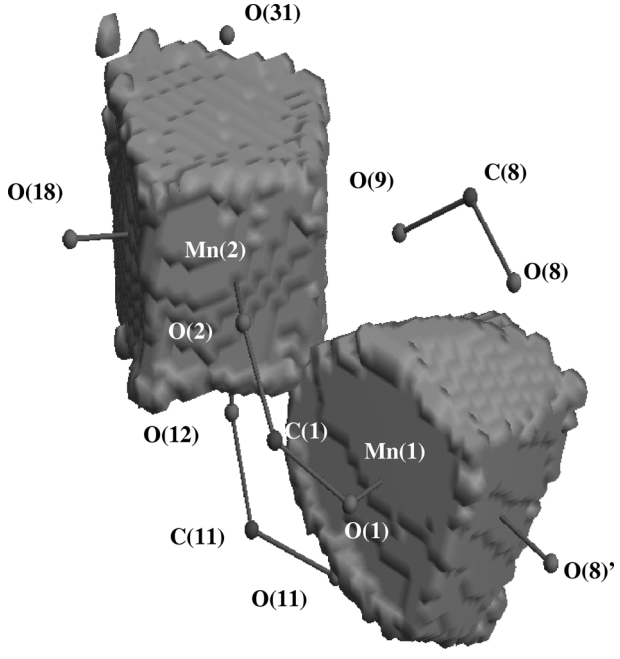

Figure 5
Atomic surfaces of the two Mn atoms, determined by topological analysis of the experimental charge density.

The authors gratefully acknowledge the provision of beam time at the ChemMatCARS beamline at the Advanced Photon Source, USA, which is funded by the NSF under grant No. CHE0087817. Use of the Advanced Photon Source was supported by the US Department of Energy, Office of Basic Energy Sciences, under Contract No. W-31-109-ENG-38. The study was supported by the DANSYNC center under the Danish Research Councils. The authors are indebted to the Carlsberg Foundation and the Danish Research Councils for funding a Quantum Design PPMS.

References

Abramov, Y. (1997). *Acta Cryst.* A**53**, 264–272.
Ashcroft, N. W. & Mermin, N. D. (1976). *Solid State Physics.* Orlando, USA: Harcourt Brace and Company.
Bader, R. F. W. (1994). *Atoms in Molecules. A Quantum Theory.* Oxford: Clarendon Press.
Bianchi, R., Gervasio, G. & Marabello, D. (2000). *Inorg. Chem.* **39**, 2360–2366.
Blessing, R. H. (1997). *J. Appl. Cryst.* **30**, 421–426.
Coppens, P. (1997). *X-ray Charge Densities and Chemical Bonding.* Oxford University Press.
Coppens, P., Iversen, B. B. & Larsen, F. K. (2004). *Coord. Chem. Rev.* In the press.
Eddaoudi, M., Kim, J., Rosi, N., Vodak, D., Wachter, J., O'Keeffe, M. & Yaghi, O. M. (2002). *Science*, **295**, 469–472.
Edgar, M., Michell, R., Slawin, A. M. Z., Lightfoot, P. & Wright, P. A. (2001). *Chem. Eur. J.* **7**, 5168–5175.
Espinosa, E., Alkorta, I., Elguero, J. & Mollins, E. (2002). *J. Chem. Phys.* **117**, 5529–5542.
Hardie, M. J., Kirschbaum, K., Martin, A. & Pinkerton, A. A. (1998). *J. Appl. Cryst.* **31**, 815–817.
Harel, M. & Hirshfeld, F. L. (1975). *Acta Cryst.* B**31**, 162–172.
Hirshfeld, F. L. (1976). *Acta Cryst.* A**32**, 239–244.
Holladay, A., Leung, P. C. & Coppens, P. (1983). *Acta Cryst.* A**39**, 377–387.
Iversen, B. B., Larsen, F. K., Pinkerton, A., Martin, A., Darovsky, A. & Reynolds, P. A. (1998). *Inorg. Chem.* **37**, 4559–4566.
Iversen, B. B., Larsen, F. K., Pinkerton, A. A., Martin, A., Darovsky, A. & Reynolds, P. A. (1999). *Acta Cryst.* B**55**, 363–374.
Kitaura, R., Kitagawa, S., Kubota, Y., Kobayashi, T. C., Kindo, K., Mita, Y., Matsuo, A., Kobayashi, M., Chang, H. C., Ozawa, T. C., Suzuki, M., Saktata, M. & Takata, M. (2003). *Science*, **298**, 2358–2361.
Koritsanszky, T., Howard, S. T., Su, Z., Mallinson, P. R., Richter, T. & Hansen, N. K. (2002). *XD.* Freie Universität Berlin, Germany.
Macchi, P., Larsen, F. K., Schultz, A. J. & Iversen, B. B. (2001). *J. Phys. Chem. A*, **105**, 9231–9242.
Macchi, P. & Sironi, A. (2003). *Coord. Chem. Rev.* **238**, 383–412.
Miller, J. S. & Epstein, A. J. (1995). *Chem. Eng. News*, **2**, 30–41.

Noro, S., Kitura, R., Kondo, M., Kitagawa, S., Ishii, T., Matsuzaka, H. & Yamashita, M. (2002). *J. Am. Chem. Soc.* **124**, 2568–2583.
O'Keeffe, M., Eddaoudi, M., Li, H., Reineke, T. & Yaghi, O. M. (2000). *J. Solid State Chem.* **152**, 3–20.
Overgaard, J., Iversen, B. B., Palii, S. P., Timco, G. A., Gerbeleu, N. V., Singerean, L. & Larsen, F. K. (2002). *Chem. Eur. J.* **8**, 2775–2786.
Overgaard, J., Larsen, F. K., Schiøtt, B. & Iversen, B. B. (2003). *J. Am. Chem Soc.* **125**, 11088–11099.
Overgaard, J., Schiøtt, B., Larsen, F. K. & Iversen, B. B. (2001). *Chem. Eur. J.* **7**, 3756–3767.
Poulsen, R. D., Bentien, A., Chevalier, M. & Iversen, B. B. (2004). In preparation.
Price, D. J., Tripp, S., Powell, A. K. & Wood, P. T. (2001). *Chem. Eur. J.* **7**, 200–208.
Rosi, N. L., Eckert, J., Eddaoudi, M., Vodak, D. T., Kim, J., O'Keefe, M. & Yaghi, O. M. (2003). *Science*, **300**, 1127–1129.
Sabino, J. R. & Coppens, P. (2003). *Acta Cryst.* A**59**, 127–131.
Sheldrick, G. M. (2003). *SMART, SAINT-Plus, SADABS* and *SHELXL*. Bruker AXS Inc., Madison, Wisconsin, USA.
Wu, G., Rodrigues, B. L. & Coppens, P. (2002). *J. Appl. Cryst.* **35**, 356–359.
Yaghi, O. M., O'Keefe, M., Ockwig, N. W., Chae, H. K., Eddaoudi, M. & Kim, J. (2003). *Nature* (*London*), **423**, 705–712.